Yang, S., Schulz, H.-M., Horsfield, B., Schovsbo, N. H., Noah, M., Panova, E., Rothe, H., Hahne, K. (2018): On the changing petroleum generation properties of Alum Shale over geological time caused by uranium irradiation. - *Geochimica et Cosmochimica Acta*, *229*, pp. 20—35.

DOI: http://doi.org/10.1016/j.gca.2018.02.049

# On the changing petroleum generation properties of Alum Shale over geological time caused by uranium irradiation

Shengyu Yang [a], Hans-Martin Schulz [a], Brian Horsfield [a], Niels H. Schovsbo [b], Mareike Noah [a], Elena Panova [c], Heike Rothe [a], Knut Hahne [a]

[a] Department of Geochemistry, Helmholtz Centre Potsdam GFZ German Research Centre for Geosciences, Telegrafenberg, D-14473 Potsdam, Germany

[b] Department of Reservoir Geology, Geological Survey of Denmark and Greenland, Øster Voldgade 10, DK-1350 Copenhagen K, Denmark

[c] Institute of Earth Sciences, Saint Petersburg State University, 7/9 Universitetskaya emb., 199034 Saint Petersburg, Russia

Corresponding author: Shengyu Yang

E-mail address: shengyuyoung@gmail.com

Tel.: 49 (0) 3312881999

# Abstract

An interdisciplinary study was carried out to unravel organic-inorganic interactions caused by the radiogenic decay of uranium in the immature organic-rich Alum Shale (Middle Cambrian-Lower Ordovician).

Based on pyrolysis experiments, uranium content is positively correlated with the gas-oil ratios and the aromaticities of both the free hydrocarbons residing in the rock and the pyrolysis products from its kerogen, indicating that irradiation has had a strong influence on organic matter composition overall and hence on petroleum potential. The Fourier Transform Ion Cyclotron Resonance mass spectrometry data reveal that macro-molecules in the uranium-rich Alum Shale samples are less alkylated than less irradiated counterparts, providing further evidence for structural alteration by α-particle bombardment. In addition, oxygen containing-compounds are enriched in the uranium-rich samples but are not easily degradable into low-molecular-weight products due to irradiation-induced crosslinking.

Irradiation has induced changes in organic matter composition throughout the shale's entire ca. 500 Ma history, irrespective of thermal history. This factor has to be taken into account when reconstructing petroleum generation history. The Alum Shale's kerogen underwent catagenesis in the main petroleum kitchen area 420 to 340 Ma bp. Our calculations suggest the kerogen was much more aliphatic and oil-prone after deposition than that after extensive exposure to radiation. In addition, the gas sorption capacity of the organic matter in the Alum Shale can be assumed to have been less developed during Palaeozoic times, in contrast to results gained by sorption experiments performed at the present day, for the same reason. The kerogen reconstruction method developed here precludes overestimations of gas generation and gas retention in the Alum Shale by taking irradiation exposure into account and can thus significantly mitigate charge risk when applied in the explorations for both conventional and unconventional hydrocarbons.



Keywords: radiolysis; Alum Shale; Uranium; predicting petroleum composition; Organic-inorganic interaction; Pyrolysis; FT-ICR MS

# 1. Introduction

The potential role played by uranium in petroleum generation, mainly through α-particle bombardment of organic matter, was recognised nearly a century ago (Lind and Bardwell, 1926). Experimental data showed that fatty acids can be decarboxylated by α particle radiation at 130$^{o}$C to form hydrocarbons (Sheppard and Burton, 1946). A correlation between uranium concentration and oil yield in the Chattanooga Shale was presented by Swanson (1960). Later, it was found that the total organic carbon (TOC) content is generally positively correlated to uranium content in petroleum source rocks (Leventhal, 1981; Swanson, 1961), and this finding is routinely applied in using spectral gamma-ray logging to delineate the occurrence of organic-rich shales (Schmoker, 1981; Serra, 1983). Uranium irradiation can also influence the characteristics of sedimentary organic matter. The reflectance of vitrinite in humic coal can be enhanced by the radiolytic effects from uranium decay (Breger, 1974). The atomic H/C and O/C ratios, which are used to define the kerogen type and thermal maturity (Durand and Espitalié, 1973), were also suggested to be affected by uranium-related irradiation (Pierce et al., 1958). Leventhal and Threlkeld (1978) showed that $^{13}C/^{12}C$ ratios are correlated to the log of the uranium concentrations, and this finding was confirmed by further investigations on shale (Dahl et al., 1988a) and bitumen samples (Court et al., 2006). Marine shale samples with high uranium contents were reported to produce pyrolysates with significantly enhanced percentages of gas and aromatic compounds compared with typical marine shales (Horsfield et al., 1992; Leventhal, 1981). Other cited effects include the decrease in aliphatic biomarker concentrations (Hoering and Navale, 1987) and modified aromatic biomarker distributions (Dahl et al., 1988a; Dahl et al., 1988b; Lewan and Buchardt, 1989) with increasing uranium contents in the shale.

While these investigations provided a fundamental understanding of the influences of uranium irradiation on petroleum generation, several key issues are still under debate.

(1) The actual processes changing Hydrogen Index (HI), Oxygen Index (OI) and $T_{max}$ in uranium-rich samples are not clear. For example, Forbes et al. (1988) and Landais (1996) reported that OI and $T_{max}$ values of vitrinite in the Akouta uranium deposit (Niger) tend to be increased by increasing uranium contents. In contrast, very low OI values have been reported for the uranium-rich Alum samples (Schulz et al., 2015), and Dahl et al. (1988a) suggested that $T_{max}$ is inversely proportional to uranium content.

(2) Possibly due to uranium depletion in response to surface weathering, no clear correlation could be found between uranium contents and the atypical pyrolysate characteristics of the Alum Shale in a

study by Horsfield et al. (1992). This led to the hypothesis that a unique algal biomolecule might be the precursor for the gas- and aromatic-rich properties (Bharati et al., 1995). Importantly, the mechanism of uranium irradiation in changing the petroleum generation potential is still a matter of debate, requiring the analysis of fresh core samples.

(3) Up until now most studies have relied heavily on artificial pyrolysis experiments to simulate the hydrocarbon generation from Alum Shale (Court et al., 2006; Dahl et al., 1988a; Horsfield et al., 1992; Leventhal, 1981), no work has been employed on the thermovaporisation which reflects the naturally generated products. It is not known whether the atypically generated hydrocarbons represent structural moieties caused by uranium irradiation or are attributable to secondary effects related to the high-temperatures and fast heating rates during pyrolysis experiments.

(4) Pyrolysis experiments based on black shale samples in their current state could provide misleading information about the petroleum potential because the kerogen structure hundreds of million years ago at the very start of the irradiation history could have been essentially different to what it is today.

The Alum Shale (Middle Cambrian – Lower Ordovician) holds the largest low-grade uranium resource in Europe. Here, we present new geochemical data on that shale which casts new light on the influence of uranium on petroleum potential. Fresh immature samples have been systematically investigated using inductively coupled plasma-mass spectrometry (ICP-MS), pyrolysis gas chromatography (Py-GC), thermovaporisation-gas chromatography (Tvap-GC), Fourier Transform Ion Cyclotron Resonance mass spectrometry (FT-ICR MS). A new method is proposed for back-calculating the aromaticity and chain length distributions of the original kerogen structure.

## 2. Study Area and Samples

The Baltic Basin covers parts of the southern Baltic Sea, the Kaliningrad Oblast, Northern Poland and the western parts of the Baltic States (Fig. 1), and contains sediments ranging in age from the Early Cambrian to the present day. The basin fill is thin in the north-eastern part and thickens toward the Teisseyre-Tornquist Zone (over 4,000 m thickness in northern Poland) (Ulmishek, 1990). Accordingly, the source rock maturity increases toward the southwest (Fig. 1).

The Alum Shale is considered to be one of the most important source rocks for oil and gas in the Baltic Basin because of its wide occurrence, considerable thicknesses and high TOC contents (Buchardt, 1999; Kotarba et al., 2014b). Named after the hydrated potassium and aluminium-bearing sulphate

113 [$KAl(SO_4)_2 \cdot 12H_2O$], the Alum Shale Formation is an informal name for Middle Cambrian, Upper
114 Cambrian (Furongian) and Lower Ordovician (Tremadocian) shale in and around the Baltic Basin
115 (Andersson, 1985; Thickpenny, 1984). This shale can be as thick as 180 metres in offshore Denmark
116 (Nielsen and Schovsbo, 2006) and 90 metres in southern Sweden (Pool et al., 2012). The TOC content
117 of the Alum Shales is typically higher than 2 wt.% (Schovsbo, 2003) and up to 22 wt.% in Middle
118 Sweden (Kosakowski et al., 2016).

119 Organic-lean grey shales are estimated to have an average uranium content of four ppm (Alloway,
120 2013; Swanson, 1960). In organic-rich marine black shales the uranium contents are higher, averaging
121 20 ppm (Swanson, 1961). However, the uranium content in the Alum Shale can be as high as 400 ppm
122 (Schovsbo, 2002). The uranium was enriched by the interaction of submarine hydrothermal activity
123 with highly anoxic waters during deposition (Berry et al., 1986; Leventhal, 1991), and this uranium
124 enrichment process was significantly enhanced by an intensified bottom water circulation at the
125 sediment/water interface (Schovsbo, 2002).

126 Thirty-four Alum Shale samples from Sweden, Estonia and Russia, covering different ages, were
127 analysed (Fig. 1). Most of the samples are from boreholes, and five samples were selected from
128 outcrops (Table 1). These samples are of low maturity according to previous maturity assessments
129 based on the reflectance of vitrinite-like macerals (Buchardt et al., 1997; Petersen et al., 2013), and
130 are thus suitable for studies of the petroleum generation potential.

# 131 3. Experimental Methods

## 132 3.1. Determination of uranium content

133 Uranium contents were measured by ICP-MS as described by Romer and Hahne (2010). About 250 mg
134 of rock powder, which had been dried at 105°C, was weighed into 15 mL teflon vials (Savillex®) and
135 decomposed using HF, Aqua Regia (3:1 mixture of 37% HCl and 63% $HNO_3$), and perchloric acid
136 ($HClO_4$). In a first step, 4 mL HF and 4 mL Aqua Regia were added to the samples. The tightly closed
137 vials were placed into a heating block (160°C) for 14 hours. After cooling, 1 mL $HClO_4$ (70%) was added
138 to destroy the organic material and fluorides. This solution was evaporated at 180°C to incipient
139 dryness. The samples were re-dissolved in 1 mL 7N $HNO_3$ and dried. Then, the $HClO_4$ step was
140 repeated twice. The samples were re-dissolved in 7N $HNO_3$ and kept at 100°C for 14 hours. This
141 solution was brought to a volume of 50 mL for analysis. Data were acquired in peak jumping mode
142 using a Galileo 4870 in pulse counting mode.

## 3.2. Thermal analysis

Rock-Eval pyrolysis and TOC measurements were performed using Rock-Eval 6 and Leco SC-632 analysers, respectively, following established procedures. Open system pyrolysis and thermovaporisation were performed using the Quantum MSSV-2 Thermal Analysis System interfaced with an Agilent GC-6890A gas chromatograph (Horsfield et al., 2014). (1) For Py-GC, about 10 mg of coarsely crushed shale was filled into a small open glass tube and heated at 300 $^{o}$C for three minutes to vent the free hydrocarbons. Hydrocarbons generated between 300 to 600 $^{o}$C, with the heating rate of 50 $^{o}$C/min, were collected and measured. Quantification of individual compounds was conducted by external standardisation with *n*-butane. (2) For Tvap-GC, around 10 mg of sample was weighed into MSSV glass capillary tubes, which were then sealed using a hydrogen flame. After introduction into the Quantum MSSV-2 Thermal Analysis System, the external surfaces of the tube were purged for five minutes at 300°C, during which time volatiles were mobilised within the tube and outer surfaces were cleaned; thereafter the tube was cracked open using a piston device to transfer the volatiles into a liquid nitrogen-cooled trap. The composition of these volatiles was quantified as described under Py-GC.

## 3.3. FT-ICR MS

Based on screening data, four representative Alum Shale samples were Soxhlet-extracted using a mixture of dichloromethane and methanol (v/v = 99:1). Mass analysis of the resulting bitumen samples was performed in negative ion Electospray Ionisation (ESI) mode with a 12 T FT-ICR mass spectrometer equipped with an Apollo II ESI source, both from Bruker Daltonik GmbH. Nitrogen was used as drying gas at a flow rate of 4.0 L/min and at a temperature of 220 °C, and also acted as nebulizing gas with 1.4 bars. The sample solutions were infused at a flow rate of 150 µL/h. The capillary voltage was set to 3000 V and an additional collision-induced dissociation voltage of 70 V in the source was applied to avoid cluster and adduct formation. Ions were accumulated in the collision cell for 0.05 s and transferred to the ICR cell within 1 ms. Spectra were recorded in broadband mode using 4 megaword data sets. For each mass spectrum, 200 scans were accumulated in a mass range from m/z 147 to 1000.

An external calibration was done using an in-house calibration mixture for ESI negative mode containing fatty acids and modified polyethylene glycols. Subsequently, each mass spectrum was internally recalibrated using known homologous series. A quadratic calibration mode was chosen for all samples. The RMS errors of the calibrations were between 0.001 and 0.031 ppm. Elemental formulae were assigned to the recalibrated m/z values with a maximal error of 0.5 ppm.

# 4. Results

## 4.1 Screening data

The uranium contents in the Alum Shale are highly variable, ranging from 11 ppm to 413 ppm (Table 1). The Middle Cambrian samples are generally lower in uranium compared with Upper Cambrian and Lower Ordovician Alum Shale samples (Table 1).

With total organic carbon (TOC) contents greater than 4.0 wt.%, except for sample UCm-9 which contains 3.0 wt.% (Table 1), most of the analysed Alum Shale samples can thus be viewed as "excellent" source rocks from the perspective of organic richness (Hunt, 1961; Peters and Cassa, 1994). The correlation between uranium and TOC contents is poor (Table 1), as also found in a more comprehensive study with more than 300 Alum Shale samples (Schovsbo, 2002).

The $T_{max}$ value of sample LO-9 from Ottenby, Southern Sweden (Fig. 1) is 441 $^{o}$C which suggests that the organic matter is early mature with respect to oil generation, whereas all other samples are immature with $T_{max}$ values lower than 430 $^{o}$C (Table 1). The maturity trend based on $T_{max}$ data is generally in accordance with the regional maturity map based on the reflectance of vitrinite-like macerals (Fig. 1). This furthermore implies that the investigated samples are not influenced by volcanic intrusions which locally occurred in Carboniferous-Permian times (Motuza et al., 1994; Obst, 2000).

In the pseudo-van Krevelen diagram, seemingly kerogen Types I, II, III, and IV occur in the Alum Shale (Fig. 2a). These kerogen classifications are, however, in conflict with the marine depositional environment of the Alum Shale (Thickpenny, 1984). Samples with low HI but high OI are mostly from a shallow well close to St. Petersburg (Russia) while the Swedish and Estonian samples are characterized by kerogen Types I and II. In general samples from the Hällekis-1 and the Saint Petersburg boreholes demonstrate inverse relationships between $T_{max}$ values and uranium contents, respectively, especially for those with uranium contents higher than 100 ppm (Fig. 2b).

## 4.2 Open pyrolysis-GC and thermovaporisation-GC

Py-GC provides an insight into the composition of kerogen in terms of moieties (Horsfield, 1989; Van de Meent et al., 1980), while the Tvap-GC documents the composition of hydrocarbons that have been generated and retained in the source rock over its geological history, minus volatile losses that have occurred during sample acquisition and storage.

Sixteen representative samples were pyrolyzed and gave significantly different pyrolysates (Table 2). The uranium-poor sample (MCm-1, U=14 ppm), which can be viewed as "typical" marine shale from the perspective of uranium concentration, generates short ($C_1$-$C_5$), intermediate- ($C_6$-$C_{14}$) and long-chained ($C_{15+}$) hydrocarbons dominated by doublets of *n*-alk-1-enes and *n*-alkanes (Fig. 3a). With increasing uranium contents, the pyrolysates contain fewer aliphatic components and are characterized by increasing contents of aromatic compounds. This can be seen for sample LO-3 (U=244 ppm) where the oil-range pyrolysates almost exclusively consist of aromatic compounds (Fig. 3). For all samples, the gas percentages and aromaticity of the pyrolysates appear to be exponentially controlled by the uranium content (Fig. 4a and b).

At least two groups can be identified when plotting the pyrolysate data in classical ternary diagrams (Fig. 5). The organic matter in all Middle Cambrian samples and in one Lower Ordovician sample (LO-9), both lean in uranium and characterised as kerogen Type II based on Rock-Eval data, have the potential to generate Paraffinic-Naphthenic-Aromatic oil with low wax contents (Fig. 5a). On the other hand, the pyrolysates generated from uranium-rich Alum Shale samples are dominated by gaseous and aromatic compounds and fall in the Type III field (Fig. 5). The presence of Type III kerogen is here ostensibly associated with either redox conditions during deposition or organic-inorganic interactions, but not to the presence of terrigenous organic matter. Because no terrestrial plant was developed as early as Lower Ordovician time and, unsurprisingly, phenol and cresol which are dominant compounds in Type III lignocellulosic terrigenous organic matter pyrolysates (Larter, 1984; Van de Meent et al., 1980) are essentially absent from the pyrolysates (Fig. 3a).

The gas to oil ratio (GOR) and the *o*-xylene/*n*-nonane ratio resulting from Tvap analyses are also proportional to uranium content (Fig. 3b and Fig. 4c and d). The high sensitivity of the Tvap derived GOR to weathering and storage conditions might partly explain some inconsistencies in the correlations. Furthermore, a GOR threshold between 5.5 and 6.9 is seemingly reached in the Tvap experiments (Fig. 4c). This value might define the maximum gas storage capacity of finely powdered samples.

## 4.3 FT-ICR MS

### 4.3.1 General elemental composition

The FT-ICR MS technique offers the ultra-high resolution detection of petroleum constituents (Hughey et al., 2001; Marshall et al., 1998) and is fundamental to the concept of "Petroleomics" (Marshall and Rodgers, 2004). FT-ICR MS run in ESI negative mode has enabled the identification of up to 30,000 NSO-containing compounds in crude oil (Bae et al., 2010), and has been widely applied in petroleum

236 science, e.g., assessments of biodegradation (Kim et al., 2005), maturity (Oldenburg et al., 2014; Poetz
237 et al., 2014), thermochemical sulphate reduction (Walters et al., 2015), migration fractionation (Liu et
238 al., 2015; Mahlstedt et al., 2016), and mineral-organic interactions (Yang and Horsfield, 2016).

239 In this study, total extracts from four representative Alum Shale samples were analysed. The relative
240 total monoisotopic ion abundance (TMIA) of each NSO class was calculated by normalizing the peak
241 area to the total area. Oxygen-containing compounds, which are mainly compounds with a hydroxyl
242 group in $O_1$ class (Walters et al., 2015) and carboxylic acids in $O_2$ class (Shi et al., 2010), are enriched in
243 the uranium-rich samples (Fig. 6) despite low OI (Table 1). Significant differences can also be found in
244 the nitrogen class distributions (Fig. 6), i.e., the nitrogen-containing group exclusively consists of the
245 $N_1$ class in the uranium-rich samples (LO-6 and UCm-1), while the $N_2$ classes only occur in the uranium-
246 poor samples (LO-9 and MCm-2).

### 247 4.3.2 Detailed $N_1$ class characterisations

248 Organic compounds containing one nitrogen atom measurable in ESI (-) FT-ICR MS are most
249 commonly the pyrrolic and indolic groups of carbazoles (Hughey et al., 2002; Pakarinen et al., 2007).
250 The double bond equivalent (DBE) is a parameter that reflects the degree of unsaturation of the
251 compounds (Stenson et al., 2003), i.e., double bonds together with aromatic and ring structures all
252 contribute to the DBE values. In the $N_1$ class, compounds with 9 DBE are carbazoles, while
253 benzocarbazoles and dibenzocarbazoles are characterized by 12 DBE and 15 DBE, respectively
254 (Hughey et al., 2002).

255 The DBE distribution of sample LO-9 extends to values that are higher than seen in the other three
256 samples, especially compounds with DBE < 9 were not detected in this sample (Fig. 7). Much more
257 pronounced differences are reflected by the carbon number distribution (Fig. 7) which denotes the
258 degree of alkylation of the core structure. The carbon numbers range to higher values in the uranium-
259 poor samples (Fig. 7a and b) compared with samples with higher uranium contents (Fig. 7c and d). In
260 the case of DBE 9, sample UCm-1 (U=155 ppm) contains up to 27 carbon numbers (Fig. 7d), which
261 means that a maximum of 15 saturated carbon atoms are attached to the core structure of carbazole
262 ($C_{12}H_9N$). In contrast, the alkylation degree for the carbazoles in sample LO-9 (U=33 ppm) is much
263 more pronounced, with carbon numbers as high as 36 (Fig. 7a).

# 5. Discussion

## 5.1 Hydrocarbon precursors and products

### 5.1.1 Kerogen structure

High uranium contents in shale have been reported as correlating with decreased atomic H/C and increased O/C ratios (Pierce et al., 1958). In the current study, the uranium content is probably not the exclusive controlling factor of the HI and OI values in the investigated samples (Fig. 2a) as OI is not necessarily high when the sample is rich in uranium (Table 1). It could be possible that the hydrocarbon potential was reduced due to the liberation of hydrogen by uranium ionising radiation (Colombo et al., 1964; Dole, 1958). However, since the original HI values of the samples are variable, a relationship between uranium contents and the current HI values could not be established.

Middle Cambrian samples and sample LO-9 with relatively low uranium contents are predicted to produce Paraffinic-Naphthenic-Aromatic Low Wax petroleum upon natural maturation, in accordance with most classical Type II marine source rocks (Horsfield, 1989). In stark contrast, the pyrolysates of the uranium-rich samples are extremely rich in gas and aromatic compounds (Fig. 5). The abundance of short-chained aliphatic compounds and alkylbenzenes can be indicative of terrigenous organic matter (Eglinton et al., 1990; Horsfield, 1989), but this does not apply here due to the Cambrian-Ordovician age of the samples. Another possible explanation could be the mineral matrix catalytic effect during pyrolysis (Espitalie et al., 1980; Horsfield and Douglas, 1980). For example, Yang et al. (2016) showed that pyrolysis on a whole rock sample of the argillaceous marine Bowland Shale (Mississippian, UK) generates much gassier and more aromatic pyrolysates than its kerogen concentrate. However, the pyrolysates of a uranium-rich Alum Shale sample before and after demineralization are identical (supplement figure), thereby ruling out this explanation.

Using the analogue that Ordovician seas were globally and uniquely populated by the alga *Gloeocapsamorpha prisca* (Fowler and Douglas, 1984), Horsfield et al. (1992) suggested that the Cambrian might also have had its own unique biota whose diagenetic residues yielded unusual pyrolysates. Bharati et al. (1995) and Sanei et al. (2014) expanded this precursor hypothesis, as algae, e.g., *Chlorella marina*, can yield aromatic-rich hydrocarbons (Derenne et al., 1996). However, the investigated Lower Ordovician samples have been documented as having similar palaeo-biota yet yield very different pyrolysates depending on the uranium contents (Fig. 4a and b). The robust correlations between uranium concentrations and key pyrolysate parameters substantiate the hypothesis that

294 irradiation is the major control of the Alum Shale products. Furthermore, pyrolysates of samples with
295 decreasing uranium contents are similar (Fig. 4a and b), leading to the conclusion that the original
296 kerogen structure of all Alum Shale samples is essentially uniform.

297 The vitrinite reflectance of humic coal increases due to the initiation and propagation of crosslinking
298 reactions by uranium irradiation, irrespective of the geological heating (Breger, 1974). Similarly,
299 Forbes et al. (1988) and Landais (1996) suggested that the $T_{max}$ of vitrinite in the Akouta uranium
300 deposit (Niger) increases when the uranium content is high. However, the inverse correlation between
301 $T_{max}$ and uranium contents observed here in the Alum Shale is in accordance with previous findings by
302 Dahl et al. (1988a). Based on molecular modelling, Claxton et al. (1993) found that the presence of
303 aromatic rings in kerogen results in a weakening of the bond energies of carbon chains, especially at
304 the ß position. This ß-cleavage of aromatic structures offers an explanation why uranium-rich samples
305 have relatively low $T_{max}$ values.

306 ### 5.1.2 Free hydrocarbons

307 The free hydrocarbons stored in the immature (low $T_{max}$) Alum Shale samples and detected by Tvap
308 may have been formed by incipient thermal cleavage reactions or by irradiation-induced maturation.
309 Jaraula et al. (2015) reported that the odd/even carbon preference of *n*-alkanes in an immature
310 deposit ($R_o$=0.26%) decreases with increasing uranium contents, and thus proposed an alternative
311 radiolytic cracking pathway of petroleum generation in addition to thermal and microbial mechanisms.
312 It is important to note that the free hydrocarbons in the Alum Shale are quantitatively limited,
313 especially from the uranium-rich samples, as revealed by the low S1 values (Table 1). Nevertheless, the
314 fit between pyrolysis results and Tvap products (Fig. 5) suggests that the uranium irradiation effect on
315 compositional variation is not limited to laboratory experiments but is also effective in nature.

316

317 ## 5.2 Heterocompounds

318 ### 5.2.1 Oxygen-containing moieties

319 The oxygen compounds in petroleum or source rock extracts can be influenced by a variety of controls
320 such as depositional environment, biodegradation, and maturity. Hughey et al. (2002) found that
321 crude oils generated from lacustrine source rocks are richer in acids ($O_2$ compounds) than crude oils
322 generated from marine source rocks. Biodegradation of oils normally raises the concentrations of
323 oxygen compounds, especially the $O_2$ class (Kim et al., 2005). Furthermore, extracts from the

Posidonia Shale (Lower Jurassic) are depleted in oxygen compounds during thermal maturation (Poetz et al., 2014).

The aforementioned factors play only a very minor role, if any, in determining the composition of oxygen-containing compounds in the Alum Shale for the following reasons: 1) The Alum Shale was deposited in a fully marine environment that predates the evolution of terrestrial plants. This implies that source type variation played a very minor role in the oxygen compound variations. 2) Samples LO-6 and UCm-1, which are borehole samples (Table 1) and therefore less prone to being biodegraded, have a high oxygen content, whereas the outcrop samples (LO-9 and MCm-2), being most susceptible to weathering effects, have low oxygen contents (Fig. 6). These together argue against surficial biodegradation. 3) Samples LO-9 and MCm-2 with similar uranium contents but very different maturities contain similar oxygen compound concentrations. This implies that the relatively small range of maturity change is not the controlling factor of elemental variabilities.

Purportedly the radiolytic cleavage of water yields highly reactive $OH^{\cdot}$ radicals which quickly react with the *in-situ* organic matter during diagenesis (Court et al., 2006; Jaraula et al., 2015), leading to enhanced oxygen contents in the kerogen structure. Alternatively, peroxides can also be formed in response of irradiation (Gebicki and Gebicki, 1993) which can further oxidize the kerogen quickly (McDonald et al., 1998). However, these oxygen-containing moieties do not degrade into low molecular weight volatiles upon pyrolysis easily, as shown by the low OI of many uranium-rich samples (Table 1 and Fig. 2a). In addition, data gained by nuclear magnetic resonance spectroscopical analyses of the Alum Shale revealed that the oxygen-bearing functional groups are still intact within the kerogen macromolecule throughout catagenesis (Bharati et al., 1995), i.e., some highly mature Alum Shale kerogens are still rich in oxygen.

### 5.2.1 Pyrrolic nitrogen-containing moieties

It is known that the average DBE in the $N_1$ class shifts toward higher values with increasing maturity for shale extracts (Poetz et al., 2014) and crude oil (Oldenburg et al., 2014) due to annulation and aromatisation. The DBE distribution in sample LO-9, which has the highest $T_{max}$ value of the four samples, could be enhanced by thermal maturation. In contrast, the other three samples have comparable maturities ($T_{max}$ values between 417 $^{o}$C to 419 $^{o}$C) and the influence of maturity can be excluded. Although the uranium-rich samples tend to generate more aromatic products during pyrolysis, the aromaticity of the bitumen is not correlated with uranium content (Fig. 7c and d).

The atomic pile (an early type of nuclear reactor) radiation of petroleum revealed that paraffins are converted into an insoluble gel after a certain dose of radiation has been reached (Charlesby, 1954). In

356 the Alum Shale, the bitumen extractability and aliphatic biomarker concentrations are inversely
357 correlated with the uranium content (Dahl et al., 1988a; Dahl et al., 1988b; Lewan and Buchardt,
358 1989). This was attributed to cross-linking and aromatisation by uranium irradiation (Hoering and
359 Navale, 1987). Similar aromatisation mechanisms of the kerogen structure in response to irradiation
360 were also proposed by Forbes et al. (1988) and Kribek et al. (1999). However, the pyrrolic nitrogen
361 compounds in the Alum Shale extracts are not obviously aromatised in the uranium-rich samples (Fig.
362 7c and d). This could imply that cross-linking, rather than aromatisation, is the primary reaction path
363 responsible for the low bitumen extractability in uranium-rich Alum Shale samples.

364 Mahlstedt et al. (2016) reported that the degree of alkylation of the $N_1$ class decreases in solvent
365 extracts of the Lower Jurassic Posidonia Shale during thermal maturation. This maturity control does
366 not serve as an explanation for the strong alkylation reduction of the two uranium-rich Alum Shale
367 samples (Fig. 7c and d) since both are immature. We deduce that it is irradiation that causes side-
368 chain cracking of alkyl chains attached to the aromatic core structures, leaving lower levels of
369 alkylation behind as a result. Similar damaging effects have been observed in the biomarker
370 distributions of the Alum Shale (Dahl et al., 1988b; Lewan and Buchardt, 1989), i.e., high molecular-
371 weight triaromatic steroids ($C_{26}$-$C_{28}$) are always absent in uranium-rich samples, this being atypical for
372 extracts of immature marine shales in general (McKenzie et al., 1983). The low alkylation degree of the
373 uranium-rich samples not only depicts the kerogen structure but may also explains why these samples
374 tend to generate gaseous products instead of long-chained compounds (Fig. 5a).

375

## 376 5.3 Kerogen structure reconstruction

### 377 5.3.1 Geological evidences for structural alteration

378 Based on its widespread occurrence, regional great thickness, and high TOC contents, the Alum Shale
379 may hold a huge unconventional gas potential (EIA, 2015). Furthermore, the Alum Shale has been
380 suggested to have a high storage capacity, based on methane adsorption measurements in the
381 laboratory of as much as 3.5 $m^3$/t (Gasparik et al., 2014). However, shale gas exploration activities in
382 southern Sweden and northern Denmark were disappointing, ostensibly due to very low gas
383 saturation (Pool et al., 2012) and possible gas leakage over geological time since tectonic movements
384 (Schovsbo et al., 2014).

385 As far as the liquid hydrocarbon potential is concerned, a very limited amount of oil with a very high
386 API gravity is anticipated to be generated from the Alum Shale based on pyrolysis experiments

(Kotarba et al., 2014a; Sanei et al., 2014). However, petrological (Schleicher et al., 1998), stable carbon isotope (Więcław et al., 2010) and biomarker (Yang et al., 2017) investigations indicate that the crude oil in Middle Cambrian sandstones and Upper Ordovician reef reservoirs in the Baltic Basin was sourced by the Alum Shale. Importantly, the produced oil was typically classified according to engineering nomenclature as "Black Oil" based on physical properties (Sivhed et al., 2004; Zdanaviciute et al., 2012). These inconsistencies imply that the composition of organic matter in the uranium-rich Alum Shale has to be evaluated carefully, with due consideration of the source rock in its present state versus that of the same shale prior to extensive radiation damage. Specifically, the kerogen in the investigated Alum Shale samples has undergone irradiation for 478-500 Myr, and must have been compositionally and structurally different from that which underwent the phase of major petroleum generation in the basin centre beginning in the Early Devonian.

### 5.3.2 Radiation dosage

The most common isotopes of natural uranium are $^{238}U$ (99.27%) and $^{235}U$ (0.72%) (Osmond and Cowart, 1976). Most of the radiation resulting from $^{238}U$ decay in natural systems is emitted in the form of α-radiation followed by less intensive γ-radiation (Jaraula et al., 2015). With a half-life of 4.5 billion years, $^{238}U$ decays exponentially (Fig. 8) and is independent of either temperature or pressure (Goodwin et al., 2009). However, the time span since the Cambrian is very short compared with the half-life, making the curvature of the exponential curve extremely small (Fig. 8). Therefore, the decay can be roughly viewed as linearly correlated with time, i.e., the rate of decay in the Alum Shale is considered constant.

Whyte (1973) proposed that the radiation dosage (D) from a point source to a detector over time (t) can be calculated by:

$$D=E\times C\times(S/4\pi r^2)\times \mu \times t$$

where E denotes the energy per decay (MeV) which is constant for $^{238}U$; C describes the activity (Bq) of decay and can also be viewed as a fixed rate as described above; S represents the area of the detector and $4\pi r^2$ is the area of a sphere with radius r, and thus the $S/4\pi r^2$ shows the probability that the radiation will reach the detector; μ is the mass energy-absorption coefficient.

Although E, C, and μ in the formula can be constant values, it is impossible to accurately measure the distance between a uranium atom and organic matter, especially the great heterogeneities of organic and inorganic matter in the shale. Nevertheless, since the uranium in Alum Shale is primarily accumulated in organic matter and phosphate nodules (Lecomte et al., 2017) and the spatial relationship of uranium and organic matter is fixed through geological time unless a metamorphism

stage is reached (Cumberland et al., 2016), it can be concluded that the radiation dosage from uranium in the sample is proportional to time. Furthermore, the cumulative effect of uranium irradiation on kerogen structure within a shale sample is linearly correlated with both uranium content and the time since shale deposition.

### 5.3.3 Kerogen reconstruction

The exponential relationships between uranium and pyrolysate parameters (Fig. 4a and b) imply that the response of kerogen structure to irradiation is not linear. A labile kerogen structure can easily be changed during the early stages; thereafter the altered structures would become less sensitive to radiation and will reach equilibrium in the end. The response curves in Fig. 4a and b describe a scenario that samples with different uranium contents have experienced a similar exposure time of irradiation. Because the uranium content and radiation time compensate with each other, these pathways should also exist when the uranium content is fixed and only radiation time varies. The irradiation dosage and the loss of $^{238}U$ is negligible since only ca. 1% of uranium would be decayed every 100 Myr.

In the case of sample UCm-2 (U=413 ppm), the pyrolysate is characterised by a gas content of 98% and an *o*-xylene content of 86% over the sum of 2,3-dimethylthiophene, *n*-nonene, and *o*-xylene (Table 2). With decreasing radiation dosage, i.e., less radiation time, the products from this shale should be less rich in gaseous and aromatic compounds. One-dimensional burial reconstructions presented by Kosakowski et al. (2010) indicate that the Alum Shale in the Baltic Basin centre started to generate and expel petroleum from the Early Devonian, e.g., the Alum Shale in well A23-1/88 (Fig. 1) was in the oil window from 420-340 Myr ago (Fig. 9). Accordingly, the compositional information on hydrocarbons generated during that time can be back-calculated, assuming that the kerogen structure in sample MCm-1 (U=14 ppm) represents the original structure of sample UCm-2 prior to irradiation. The gas and *o*-xylene contents are calculated as 88-91% and 66-73 %, respectively (Fig. 9), which are still high for typical marine shales (Fig. 5). When petroleum generation started in Devonian times, the Alum Shale had experienced about 1/5 of the total exposure to radiation compared with samples today, but the extent of kerogen alteration was more advanced, due to the exponential response of the kerogen structure to irradiation dosage. This method can also be applied to samples with lower uranium contents, and the products inferred to have formed back in Palaeozoic times must have been more oil-rich and aliphatic than those from sample UCm-2.

### 5.3.4 Further implications

Ziegs et al. (2017) reported that the ability of shale to retain light hydrocarbons is proportional to the aromaticity of its labile kerogen, and therefore, the gas adsorption capacity of the Alum Shale over geological time could have also been overestimated. The expected highest risks of gas leaks from the Alum Shale are assumed to have occurred during late Caledonian orogeny, the Carboniferous uplift, and the Neogene uplift (Pool et al., 2012; Schovsbo et al., 2014). When those tectonic movements happened, the gas retention capacity of the Alum Shale kerogen would have been much smaller than the values suggested by adsorption experiments and much more gas could have been lost as a result of the tectonic uplifts than previously thought. Therefore, the experimental data based on the Alum Shale samples today should only be used as the upper limit of gas adsorption capacity in resource estimates.

The uranium irradiation effects causing changes in the distribution of triaromatic steroids biomarkers (Dahl et al., 1988b; Lewan and Buchardt, 1989) can be applied in oil-source rock correlation. Yang et al. (2017) proposed that oil with low $C_{26}$–$C_{28}$ triaromatic steroids was sourced from uranium-rich Alum Shale (UCm-4 and MCm-1 are shown as Kak/a and Kak/b, respectively, in their Fig. 5). As stated above, the kerogen structure of UCm-4 (U=231 ppm) was partly altered by uranium irradiation. However, the $C_{26}$–$C_{28}$ triaromatic steroids were already completely removed (Yang et al., 2017). Similarly, an Alum Shale sample with 163 ppm uranium (sample B26, Fig. 9 in Dahl et al. (1988b)) was totally depleted in high-molecular triaromatic steroids. These overall findings imply that the soluble aromatic biomarkers are much more sensitive to uranium irradiation than the solid kerogen structure.

In addition, the changes in organic matter composition in response to irradiation as outlined here can also be instructive for extra-terrestrial research in which strong radiation is ubiquitous (Allen et al., 1998), and also for the evaluation of the long-term impact of uranium waste disposal in shales (Gautschi, 2001).

## 6. Conclusions

1. Neither the HI nor the OI of immature Alum Shale is correlated with uranium contents. The HI could be decreased by uranium irradiation, but the diverse original HI values prevent any correlation. Oxygen compounds are enriched by the existence of uranium but are mainly intact in kerogen macromolecules.

2. Most of the Alum Shale samples generate gas-rich and aromatic products through pyrolysis experiments which are atypical for marine shales. Gas and *o*-xylene percentages in pyrolysates and natural products are both proportional to uranium contents, suggesting that irradiation strongly alters kerogen structure.

3. The irradiation does not significantly increase the aromatisation of macromolecules. Instead, the average chain lengths of alkyl substituents bound to aromatic structures was shortened by the irradiation bombardment and is responsible for the high potential for gas generation.

4. Both uranium contents and exposure time are linearly correlated with uranium radiation dosage. However, the response of kerogen structure to radiation is exponential, because the labial structures are altered in the early stages of irradiation.

5. About half of the irradiation-induced kerogen changes occurred when the Alum Shale was at an oil-window maturity. The back-calculation of the kerogen structure can avoid over-estimations of gas generation and retention of the Alum Shale.

# Acknowledgment

We thank Gripen Oil & Gas AB and the Geological Survey of Sweden for providing the samples. Nicolaj Mahlstedt is acknowledged for fruitful discussions. Kind thanks are extended to Ferdinand Perssen and Cornelia Karger for their technical support. This study is financially supported by the Chinese Scholarship Council for S. Yang.

# Reference


Allen, R.G., Pereira, L.S., Raes, D. and Smith, M. (1998) Crop evapotranspiration-Guidelines for computing crop water requirements-FAO Irrigation and drainage paper 56. FAO, Rome 300, D05109.

Alloway, B.J. (2013) Bioavailability of elements in soil, in: Selinus, O. (Ed.), Essentials of medical geology. Springer, Dordrecht, pp. 351-373.

Andersson, A. (1985) The Scandinavian alum shales. Sveriges geologiska undersökning, Uppsala, Sweden.

Bae, E., Na, J.-G., Chung, S.H., Kim, H.S. and Kim, S. (2010) Identification of about 30 000 Chemical Components in Shale Oils by Electrospray Ionization (ESI) and Atmospheric Pressure Photoionization (APPI) Coupled with 15 T Fourier Transform Ion Cyclotron Resonance Mass Spectrometry (FT-ICR MS) and a Comparison to Conventional Oil. Energy & Fuels 24, 2563-2569.

Berry, W.B., Wilde, P., Quinby-Hunt, M.S. and Orth, C.J. (1986) Trace element signatures in Dictyonema Shales and their geochemical and stratigraphic significance. Norsk Geol. Tidsskr 66, 45-51.

Bharati, S., Patience, R.L., Larter, S.R., Standen, G. and Poplett, I.J.F. (1995) Elucidation of the Alum Shale kerogen structure using a multi-disciplinary approach. Organic Geochemistry 23, 1043-1058.

Breger, I. (1974) The role of organic matter in the accumulation of uranium: the organic geochemistry of the coal-uranium association. Formation of uranium ore deposits, 99-124.

Buchardt, B. (1999) Gas Potential of the Cambro-Ordovician Alum Shale in Southern Scandinavia and the Baltic Region. Geologische Jahrbuch, 9-24.

Buchardt, B., Nielsen, A.T., Schovsbo, N.H. and Bojesen-Kofoed, J. (1997) Alun skiferen i Skandinavien. Geologisk Tidsskrift 1997, 1-30.

Charlesby, A. (1954) The cross-linking and degradation of paraffin chains by high-energy radiation, Proceedings of the Royal Society of London A: Mathematical, Physical and Engineering Sciences. The Royal Society, pp. 60-74.

Claxton, M., Patience, R. and Park, P. (1993) Molecular modelling of bond energies in potential kerogen sub-units, Extended Abstracts of the 16th International Meeting on Organic Geochemistry. Falch Hurtigtrykk, Oslo, Stavanger, pp. 198-201.

Colombo, U., Sironi, G. and Denti, E. (1964) A geochemical investigation upon the effects of ionizing radiation on hydrocarbons. J. Inst. Petrol. 50.

Court, R.W., Sephton, M.A., Parnell, J. and Gilmour, I. (2006) The alteration of organic matter in response to ionising irradiation: Chemical trends and implications for extraterrestrial sample analysis. Geochimica et Cosmochimica Acta 70, 1020-1039.

Cumberland, S.A., Douglas, G., Grice, K. and Moreau, J.W. (2016) Uranium mobility in organic matter-rich sediments: A review of geological and geochemical processes. Earth-Science Reviews 159, 160-185.

Dahl, J., Hallberg, R. and Kaplan, I. (1988a) The effects of radioactive decay of uranium on elemental and isotopic ratios of Alum Shale kerogen. Applied Geochemistry 3, 583-589.

Dahl, J., Hallberg, R. and Kaplan, I.R. (1988b) Effects of irradiation from uranium decay on extractable organic matter in the Alum Shales of Sweden. Organic Geochemistry 12, 559-571.

Derenne, S., Largeau, C. and Berkaloff, C. (1996) First example of an algaenan yielding an aromatic-rich pyrolysate. Possible geochemical implications on marine kerogen formation. Organic Geochemistry 24, 617-627.

Dole, M. (1958) The Effects of Ionizing Radiation on Natural and Synthetic High Polymers. J Am Chem Soc 80, 6694-6694.

546 Durand, B. and Espitalié, J. (1973) Evolution de la matière organique au cours de
547 l'enfouissement des sédiments. Compte rendus de l'Académie des Sciences (Paris) 276, 2253-
548 2256.
549 Eglinton, T.I., Damste, J.S.S., Kohnen, M.E.L. and Deleeuw, J.W. (1990) Rapid Estimation of the
550 Organic Sulfur-Content of Kerogens, Coals and Asphaltenes by Pyrolysis-Gas Chromatography.
551 Fuel 69, 1394-1404.
552 EIA (2015) Technically Recoverable Shale Oil and Shale Gas Resources.
553 Espitalie, J., Madec, M. and Tissot, B. (1980) Role of mineral matrix in kerogen pyrolysis:
554 influence on petroleum generation and migration. AAPG Bulletin 64, 59-66.
555 Espitalie, J., Madec, M., Tissot, B., Mennig, J. and Leplat, P. (1977) Source rock characterization
556 method for petroleum exploration, The 9th Annual Offshore Technology Conference. Offshore
557 Technology Conference, Houston, Texas, pp. 439-444.
558 Forbes, P., Landais, P., Bertrand, P., Brosse, E., Espitalie, J. and Yahaya, M. (1988) Chemical
559 transformations of type-III organic matter associated with the Akouta uranium deposit
560 (Niger): geological implications. Chemical geology 71, 267-282.
561 Fowler, M. and Douglas, A. (1984) Distribution and structure of hydrocarbons in four organic-
562 rich Ordovician rocks. Organic Geochemistry 6, 105-114.
563 Gasparik, M., Bertier, P., Gensterblum, Y., Ghanizadeh, A., Krooss, B.M. and Littke, R. (2014)
564 Geological controls on the methane storage capacity in organic-rich shales. International
565 Journal of Coal Geology 123, 34-51.
566 Gautschi, A. (2001) Hydrogeology of a fractured shale (Opalinus Clay): Implications for deep
567 geological disposal of radioactive wastes. Hydrogeol J 9, 97-107.
568 Gebicki, S. and Gebicki, J.M. (1993) Formation of peroxides in amino acids and proteins
569 exposed to oxygen free radicals. Biochem J 289, 743-749.
570 Goodwin, J.R., Golovko, V.V., Iacob, V.E. and Hardy, J.C. (2009) Half-life of the electron-
571 capture decay of Ru-97: Precision measurement shows no temperature dependence. Phys Rev
572 C 80, 045501.
573 Hoering, T.C. and Navale, V. (1987) A search for molecular fossils in the kerogen of
574 Precambrian sedimentary rocks. Precambrian Res 34, 247-267.
575 Horsfield, B. (1989) Practical criteria for classifying kerogens: some observations from
576 pyrolysis-gas chromatography. Geochimica et Cosmochimica Acta 53, 891-901.
577 Horsfield, B., Bharati, S. and Larter, S.R. (1992) On the atypical petroleum-generating
578 characteristics of alginite in the Cambrian Alum Shale, in: Schidlowski, M., Golubic, S.,
579 Kimberley, M.M., Sr, D.M.M., Trudinger, P.A. (Eds.), Early Organic Evolution. Springer Berlin
580 Heidelberg, pp. 257-266.
581 Horsfield, B. and Douglas, A. (1980) The influence of minerals on the pyrolysis of kerogens.
582 Geochimica et Cosmochimica Acta 44, 1119-1131.
583 Horsfield, B., Leistner, F. and Hall, K. (2014) Microscale sealed vessel pyrolysis. Principles and
584 Practice of Analytical Techniques in Geosciences 4, 209.
585 Hughey, C.A., Hendrickson, C.L., Rodgers, R.P., Marshall, A.G. and Qian, K. (2001) Kendrick
586 mass defect spectrum: a compact visual analysis for ultrahigh-resolution broadband mass
587 spectra. Anal Chem 73, 4676-4681.
588 Hughey, C.A., Rodgers, R.P., Marshall, A.G., Qian, K.N. and Robbins, W.K. (2002)
589 Identification of acidic NSO compounds in crude oils of different geochemical origins by
590 negative ion electrospray Fourier transform ion cyclotron resonance mass spectrometry.
591 Organic Geochemistry 33, 743-759.
592 Hunt, J.M. (1961) Distribution of hydrocarbons in sedimentary rocks. Geochimica et
593 cosmochimica Acta 22, 37-49.
594 Jaraula, C.M.B., Schwark, L., Moreau, X., Pickel, W., Bagas, L. and Grice, K. (2015) Radiolytic
595 alteration of biopolymers in the Mulga Rock (Australia) uranium deposit. Applied
596 Geochemistry 52, 97-108.
597 Kim, S., Stanford, L.A., Rodgers, R.P., Marshall, A.G., Walters, C.C., Qian, K., Wenger, L.M. and
598 Mankiewicz, P. (2005) Microbial alteration of the acidic and neutral polar NSO compounds

revealed by Fourier transform ion cyclotron resonance mass spectrometry. Organic Geochemistry 36, 1117-1134.
Kosakowski, P., Kotarba, M.J., Piestrzyński, A., Shogenova, A. and Więcław, D. (2016) Petroleum source rock evaluation of the Alum and Dictyonema Shales (Upper Cambrian–Lower Ordovician) in the Baltic Basin and Podlasie Depression (eastern Poland). International Journal of Earth Sciences 106, 743-761.
Kosakowski, P., Wrobel, M. and Poprawa, P. (2010) Hydrocarbon generation and expulsion modelling of the lower Paleozoic source rocks in the Polish part of the Baltic region. Geological Quarterly 54, 241-256.
Kotarba, M., Lewan, M. and Więcław, D. (2014a) Shale Gas and Oil Potential of Lower Palaeozoic Strata in the Polish Baltic Basin by Hydrous Pyrolysis, Fourth EAGE Shale Workshop. EAGE, Porto, Portugal, pp. 1-5.
Kotarba, M.J., Wieclaw, D., Dziadzio, P., Kowalski, A., Kosakowski, P. and Bilkiewicz, E. (2014b) Organic geochemical study of source rocks and natural gas and their genetic correlation in the eastern part of the Polish Outer Carpathians and Palaeozoic-Mesozoic basement. Marine and Petroleum Geology 56, 97-122.
Kribek, B., Zak, K., Spangenberg, J., Jehlicka, J., Prokes, S. and Kominek, J. (1999) Bitumens in the late Variscan hydrothermal vein-type uranium deposit of Pribram, Czech Republic: Sources, radiation-induced alteration, and relation to mineralization. Econ Geol Bull Soc 94, 1093-1114.
Landais, P. (1996) Organic geochemistry of sedimentary uranium ore deposits. Ore Geol Rev 11, 33-51.
Larter, S. (1984) Application of analytical pyrolysis techniques to kerogen characterization and fossil fuel exploration/exploitation, Analytical pyrolysis. Butterworths London, pp. 212-272.
Lecomte, A., Cathelineau, M., Michels, R., Peiffert, C. and Brouand, M. (2017) Uranium mineralization in the Alum Shale Formation (Sweden): Evolution of a U-rich marine black shale from sedimentation to metamorphism. Ore Geol Rev 88, 71-98.
Leventhal, J. (1991) Comparison of organic geochemistry and metal enrichment in two black shales: Cambrian Alum Shale of Sweden and Devonian Chattanooga Shale of United States. Mineralium Deposita 26, 104-112.
Leventhal, J.S. (1981) Pyrolysis gas chromatography-mass spectrometry to characterize organic matter and its relationship to uranium content of Appalachian Devonian black shales. Geochimica et Cosmochimica Acta 45, 883-889.
Leventhal, J.S. and Threlkeld, C.N. (1978) Carbon-13/carbon-12 isotope fractionation of organic matter associated with uranium ores induced by alpha irradiation. Science 202, 430-432.
Lewan, M.D. and Buchardt, B. (1989) Irradiation of organic matter by uranium decay in the Alum Shale, Sweden. Geochimica et Cosmochimica Acta 53, 1307-1322.
Lind, S. and Bardwell, D. (1926) The chemical action of gaseous ions produced by alpha particles. IX. Saturated hydrocarbons. J Am Chem Soc 48, 2335-2351.
Liu, P., Li, M.W., Jiang, Q.G., Cao, T.T. and Sun, Y.G. (2015) Effect of secondary oil migration distance on composition of acidic NSO compounds in crude oils determined by negative-ion electrospray Fourier transform ion cyclotron resonance mass spectrometry. Organic Geochemistry 78, 23-31.
Mahlstedt, N., Horsfield, B., Wilkes, H. and Poetz, S. (2016) Tracing the Impact of Fluid Retention on Bulk Petroleum Properties Using Nitrogen-Containing Compounds. Energy & Fuels 30, 6290-6305.
Marshall, A.G., Hendrickson, C.L. and Jackson, G.S. (1998) Fourier transform ion cyclotron resonance mass spectrometry: a primer. Mass Spectrom Rev 17, 1-35.
Marshall, A.G. and Rodgers, R.P. (2004) Petroleomics: the next grand challenge for chemical analysis. Acc Chem Res 37, 53-59.
McDonald, G.D., de Vanssay, E. and Buckley, J.R. (1998) Oxidation of organic macromolecules by hydrogen peroxide: implications for stability of biomarkers on Mars. Icarus 132, 170-175.
McKenzie, D., Mackenzie, A.S., Maxwell, J.R. and Sajgo, C. (1983) Isomerization and aromatization of hydrocarbons in stretched sedimentary basins. Nature 301, 504-506.

652 Motuza, G., Kepezinskas, P. and Šliaupa, S. (1994) Diabases from the well D-1 in the Baltic Sea.
653 Geologija 16, 16-20.
654 Nielsen, A.T. and Schovsbo, N.H. (2006) Cambrian to basal Ordovician lithostratigraphy in
655 southern Scandinavia. Bulletin of the Geological Society of Denmark 53, 47-92.
656 Obst, K. (2000) Permo-Carboniferous dyke magmatism on the Danish island Bornholm. Neues
657 Jahrbuch Fur Geologie Und Palaontologie-Abhandlungen 218, 243-266.
658 Oldenburg, T.B.P., Brown, M., Bennett, B. and Larter, S.R. (2014) The impact of thermal
659 maturity level on the composition of crude oils, assessed using ultra-high resolution mass
660 spectrometry. Organic Geochemistry 75, 151-168.
661 Osmond, J. and Cowart, J. (1976) The theory and uses of natural uranium isotopic variations in
662 hydrology. Atomic Energy Review 14, 621-679.
663 Pakarinen, J.M.H., Teravainen, M.J., Pirskanen, A., Wickstrom, K. and Vainiotalo, P. (2007) A
664 positive-ion electrospray ionization Fourier transform ion cyclotron resonance mass
665 spectrometry study of Russian and north sea crude oils and their six distillation fractions.
666 Energy & Fuels 21, 3369-3374.
667 Peters, K.E. and Cassa, M.R. (1994) Applied source rock geochemistry, in: Magoon, L.B., Dow,
668 W.G. (Eds.), The Petroleum System--From Source to Trap. American Association of Petroleum
669 Geologists, pp. 93-120.
670 Petersen, H.I., Schovsbo, N.H. and Nielsen, A.T. (2013) Reflectance measurements of zooclasts
671 and solid bitumen in Lower Paleozoic shales, southern Scandinavia: Correlation to vitrinite
672 reflectance. International Journal of Coal Geology 114, 1-18.
673 Pierce, A.P., Mytton, J.W. and Barnett, P.R. (1958) Geochemistry of uranium in organic
674 substances in petroliferous rocks, Second. United Nations International Conference on the
675 Peaceful Uses of Atomic Energy. United Nation, Geneva, Switzerland, pp. 192-198.
676 Poetz, S., Horsfield, B. and Wilkes, H. (2014) Maturity-Driven Generation and Transformation
677 of Acidic Compounds in the Organic-Rich Posidonia Shale as Revealed by Electrospray
678 Ionization Fourier Transform Ion Cyclotron Resonance Mass Spectrometry. Energy & Fuels 28,
679 4877-4888.
680 Pool, W., Geluk, M., Abels, J., Tiley, G., Idiz, E. and Leenaarts, E. (2012) Assessment of an
681 unusual European shale gas play: the Cambro-Ordovician alum shale, southern Sweden,
682 SPE/EAGE European Unconventional Resources Conference and Exhibition. Society of
683 Petroleum Engineers, Vienna, Austria, pp. 1-12.
684 Romer, R.L. and Hahne, K. (2010) Life of the Rheic Ocean: Scrolling through the shale record.
685 Gondwana Res 17, 236-253.
686 Sanei, H., Petersen, H.I., Schovsbo, N.H., Jiang, C. and Goodsite, M.E. (2014) Petrographic and
687 geochemical composition of kerogen in the Furongian (U.Cambrian) Alum Shale, central
688 Sweden: Reflections on the petroleum generation potential. International Journal of Coal
689 Geology 132, 158-169.
690 Schleicher, M., Koster, J., Kulke, H. and Weil, W. (1998) Reservoir and source-rock
691 characterisation of the early palaeozoic interval in the peribaltic syneclise, northern Poland.
692 Journal of Petroleum Geology 21, 33-56.
693 Schmoker, J.W. (1981) Determination of organic-matter content of Appalachian Devonian
694 shales from gamma-ray logs. AAPG Bulletin 65, 1285-1298.
695 Schovsbo, N.H. (2002) Uranium enrichment shorewards in black shales: A case study from the
696 Scandinavian Alum Shale. Journal of the Geological Society of Sweden 124, 107-115.
697 Schovsbo, N.H. (2003) The geochemistry of Lower Palaeozoic sediments deposited on the
698 margins of Baltica. Bulletin of the Geological Society of Denmark 50, 11-27.
699 Schovsbo, N.H., Nielsen, A.T. and Gautier, D.L. (2014) The Lower Palaeozoic shale gas play in
700 Denmark. Geological Survey of Denmark and Greenland Bulletin 31, 19-22.
701 Schulz, H.M., Biermann, S., van Berk, W., Kruger, M., Straaten, N., Bechtel, A., Wirth, R.,
702 Luders, V., Schovsbo, N.H. and Crabtree, S. (2015) From shale oil to biogenic shale gas:
703 Retracing organic-inorganic interactions in the Alum Shale (Furongian-Lower Ordovician) in
704 southern Sweden. AAPG Bulletin 99, 927-956.

705 Serra, O. (1983) Fundamentals of well-log interpretation. Elsevier Science Pub. Co., Inc., New
706 York, United States.
707 Sheppard, C.W. and Burton, V.L. (1946) The Effects of Radioactivity on Fatty Acids1, 1a. J Am
708 Chem Soc 68, 1636-1639.
709 Shi, Q.A., Zhao, S.Q., Xu, Z.M., Chung, K.H., Zhang, Y.H. and Xu, C.M. (2010) Distribution of
710 Acids and Neutral Nitrogen Compounds in a Chinese Crude Oil and Its Fractions:
711 Characterized by Negative-Ion Electrospray Ionization Fourier Transform Ion Cyclotron
712 Resonance Mass Spectrometry. Energy & Fuels 24, 4005-4011.
713 Sivhed, U., Erlstrom, M., Bojesen-Koefoed, J.A. and Lofgren, A. (2004) Upper Ordovician
714 carbonate mounds on Gotland, central Baltic Sea: Distribution, composition and reservoir
715 characteristics. Journal of Petroleum Geology 27, 115-140.
716 Stenson, A.C., Marshall, A.G. and Cooper, W.T. (2003) Exact masses and chemical formulas of
717 individual Suwannee River fulvic acids from ultrahigh resolution electrospray ionization
718 Fourier transform ion cyclotron resonance mass spectra. Anal Chem 75, 1275-1284.
719 Swanson, V.E. (1960) Oil yield and uranium content of black shales. U.S. Atomic Energy
720 Commission, Washington, US.
721 Swanson, V.E. (1961) Geology and geochemistry of uranium in marine black shales: a review.
722 U.S. Atomic Energy Commission, Washington, US.
723 Thickpenny, A. (1984) The sedimentology of the Swedish Alum Shales. Geological Society,
724 London, Special Publications 15, 511-525.
725 Ulmishek, G. (1990) Geologic evolution and petroleum resources of the Baltic Basin, in:
726 Leighton, M.W., Kolata, D.R., Oltz, D.F., Eidel, J.J. (Eds.), Interior Cratonic Basins. American
727 Association of Petroleum Geologists, Tulsa, Oklahoma, pp. 603-632.
728 Van de Meent, D., Brown, S.C., Philp, R.P. and Simoneit, B.R. (1980) Pyrolysis-high resolution
729 gas chromatography and pyrolysis gas chromatography-mass spectrometry of kerogens and
730 kerogen precursors. Geochimica et Cosmochimica Acta 44, 999-1013.
731 Walters, C.C., Wang, F.C., Qian, K.N., Wu, C.P., Mennito, A.S. and Wei, Z.B. (2015) Petroleum
732 alteration by thermochemical sulfate reduction - A comprehensive molecular study of aromatic
733 hydrocarbons and polar compounds. Geochimica et Cosmochimica Acta 153, 37-71.
734 Whyte, G.N. (1973) Principles of radiation dosimetry. John Wiley and Sons, Inc., New York.
735 Więcław, D., Kotarba, M.J. and Kowalski, A. (2010) Origin of oils accumulated in the Middle
736 Cambrian reservoirs of the Polish part of the Baltic region. Geological Quarterly 54, 205-216.
737 Yang, S. and Horsfield, B. (2016) Some predicted effects of minerals on the generation of
738 petroleum in nature. Energy & Fuels 30, 6677-6687.
739 Yang, S., Horsfield, B., Mahlstedt, N., Stephenson, M. and Konitzer, S. (2016) On the primary
740 and secondary petroleum generating characteristics of the Bowland Shale, northern England.
741 Journal of the Geological Society 173, 292-305.
742 Yang, S., Schulz, H.-M., Schovsbo, N.H. and Bojesen-Koefoed, J.A. (2017) Oil-source rock
743 correlation of the Lower Palaeozoic petroleum system in the Baltic Basin (northern Europe).
744 AAPG Bulletin preliminary version published online Ahead of Print May 22, 2017.
745 Zdanaviciute, O., Lazauskiene, J., Khoubldikov, A.I., Dakhnova, M.V. and Zheglova, T.P. (2012)
746 The Middle Cambrian Succession in the Central Baltic Basin: Geochemistry of Oils and
747 Sandstone Reservoir Characteristics. Journal of Petroleum Geology 35, 237-254.
748 Ziegs, V., Horsfield, B., Skeie, J.E. and Rinna, J. (2017) Petroleum retention in the Mandal
749 Formation, Central Graben, Norway. Marine and Petroleum Geology 83, 195-214.

750

751

# Tables and Figures:

Table 1. Background information, uranium contents, and Rock-Eval and TOC data of the Alum Shale samples.

| Age | Name | Type | Well/Place | Uranium Content (ppm) | TOC (%) | Rock-Eval | | | | |
|---|---|---|---|---|---|---|---|---|---|---|
| | | | | | | S1 (mg/g) | S2 (mg/g) | $T_{max}$ (°C) | HI (mg HC/g TOC) | OI (mg $CO_2$/g TOC) |
| Lower Ordovician | LO-1 | borehole | Saint Petersburg | 74 | 11.1 | 0.3 | 23.7 | 409 | 214 | 33 |
| | LO-2 | borehole | Saint Petersburg | 190 | 9.0 | 0.3 | 17.6 | 412 | 195 | 31 |
| | LO-3 | borehole | Saint Petersburg | 244 | 13.6 | 0.4 | 21.9 | 411 | 161 | 30 |
| | LO-4 | borehole | Saint Petersburg | 274 | 6.2 | 0.2 | 5.9 | 414 | 95 | 47 |
| | LO-5 | borehole | Saint Petersburg | 110 | 9.4 | 0.1 | 8.4 | 419 | 59 | 37 |
| | LO-6 | borehole | NA-3 | 136 | 14.1 | 0.8 | 53.6 | 419 | 380 | 2 |
| | LO-7 | borehole | F-342 | 107 | 8.1 | 0.3 | 33.8 | 406 | 416 | 2 |
| | LO-8 | borehole | P-1949 | 119 | 12.4 | 2.5 | 47.6 | 405 | 385 | 3 |
| | LO-9 | outcrop | Ottenby | 33 | 8.1 | 0.6 | 30.1 | 441 | 374 | 0 |
| Upper Cambrian | UCm-1 | borehole | OA-1 | 155 | 16.7 | 1.0 | 59.6 | 417 | 387 | 1 |
| | UCm-2 | borehole | GH-2B | 413 | 21.7 | 1.3 | 73.4 | 426 | 338 | 2 |
| | UCm-3 | borehole | KN-1A | 135 | 13.1 | 1.9 | 50.5 | 425 | 385 | 1 |
| | UCm-4 | outcrop | Kakeled | 186 | 21.7 | 2.2 | 83.4 | 416 | 384 | 2 |
| | UCm-5 | outcrop | Kakeled | 194 | 11.1 | 0.6 | 42.2 | 418 | 381 | 1 |
| | UCm-6 | borehole | Hällekis-1 | 201 | 11.6 | 1.4 | 57.4 | 413 | 497 | 10 |
| | UCm-7 | borehole | Hällekis-1 | 177 | 14.6 | 1.0 | 53.1 | 417 | 365 | 8 |
| | UCm-8 | borehole | Hällekis-1 | 50 | 4.1 | 0.2 | 11.6 | 420 | 284 | 20 |
| | UCm-9 | borehole | Hällekis-1 | 142 | 3.0 | 0.5 | 8.8 | 419 | 298 | 30 |
| | UCm-10 | borehole | Hällekis-1 | 130 | 14.0 | 0.9 | 60.9 | 420 | 435 | 11 |
| | UCm-11 | borehole | Hällekis-1 | 109 | 12.6 | 0.9 | 59.0 | 420 | 467 | 12 |
| | UCm-12 | borehole | Hällekis-1 | 97 | 13.4 | 0.9 | 64.1 | 421 | 479 | 10 |
| | UCm-13 | borehole | Hällekis-1 | 84 | 22.1 | 1.9 | 138.1 | 426 | 624 | 5 |
| | UCm-14 | borehole | Hällekis-1 | 87 | 10.7 | 1.3 | 52.2 | 424 | 490 | 10 |
| Middle Cambrian | MCm-1 | outcrop | N. Djupvik | 14 | 9.9 | 1.8 | 33.4 | 421 | 338 | 4 |
| | MCm-2 | outcrop | Kakeled | 35 | 13.5 | 2.0 | 47.7 | 418 | 353 | 2 |
| | MCm-3 | borehole | Hällekis-1 | 21 | 11.1 | 2.5 | 59.8 | 423 | 537 | 10 |
| | MCm-4 | borehole | Hällekis-1 | 35 | 11.1 | 3.9 | 56.6 | 420 | 511 | 4 |
| | MCm-5 | borehole | Hällekis-1 | 35 | 10.8 | 2.1 | 21.1 | 423 | 195 | 9 |
| | MCm-6 | borehole | Hällekis-1 | 43 | 11.3 | 3.2 | 77.3 | 426 | 686 | 7 |
| | MCm-7 | borehole | Hällekis-1 | 47 | 22.0 | 2.7 | 128.4 | 423 | 583 | 6 |
| | MCm-8 | borehole | Hällekis-1 | 44 | 10.4 | 2.9 | 52.8 | 416 | 508 | 7 |
| | MCm-9 | borehole | Hällekis-1 | 34 | 12.2 | 4.3 | 55.0 | 418 | 451 | 6 |
| | MCm-10 | borehole | Hällekis-1 | 11 | 3.3 | 1.4 | 16.3 | 426 | 498 | 14 |
| | MCm-11 | borehole | Hällekis-1 | 22 | 5.9 | 1.8 | 31.3 | 422 | 529 | 14 |

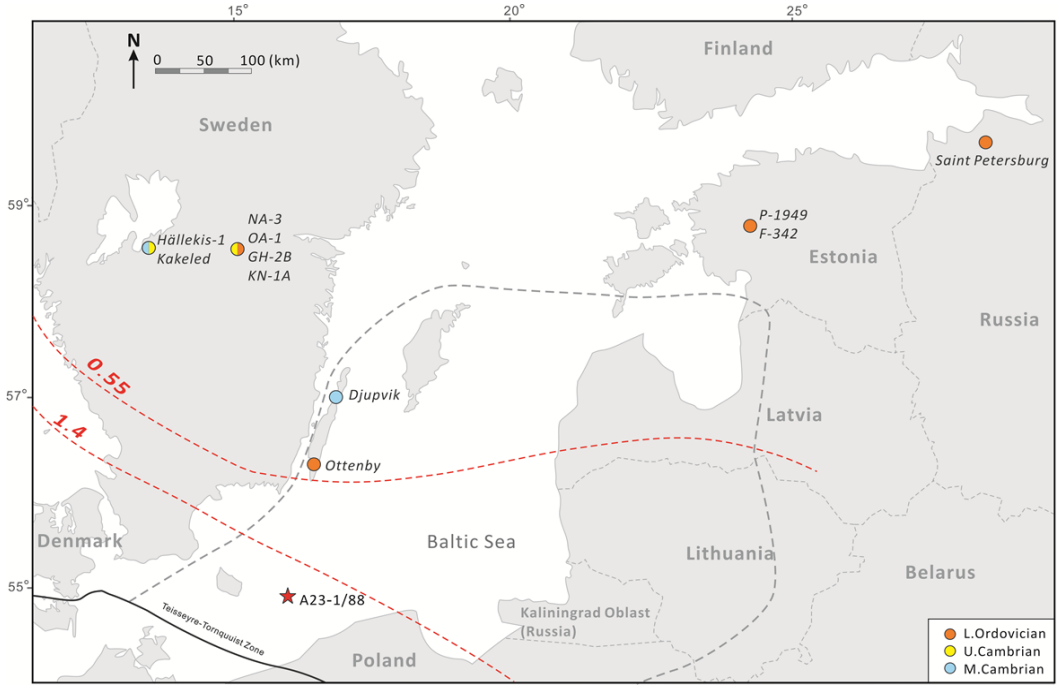


Fig. 1. Geographical overview of the Alum Shale sample distribution. The grey dashed line depicts the boundary of the Baltic Basin, and the red dashed lines represent the isolines of vitrinite-like maceral reflectance of the Alum Shale, modified after Buchardt et al. (1997). Ages of the samples are given in coloured circles. The red star denotes the well for 1-D basin modeling.

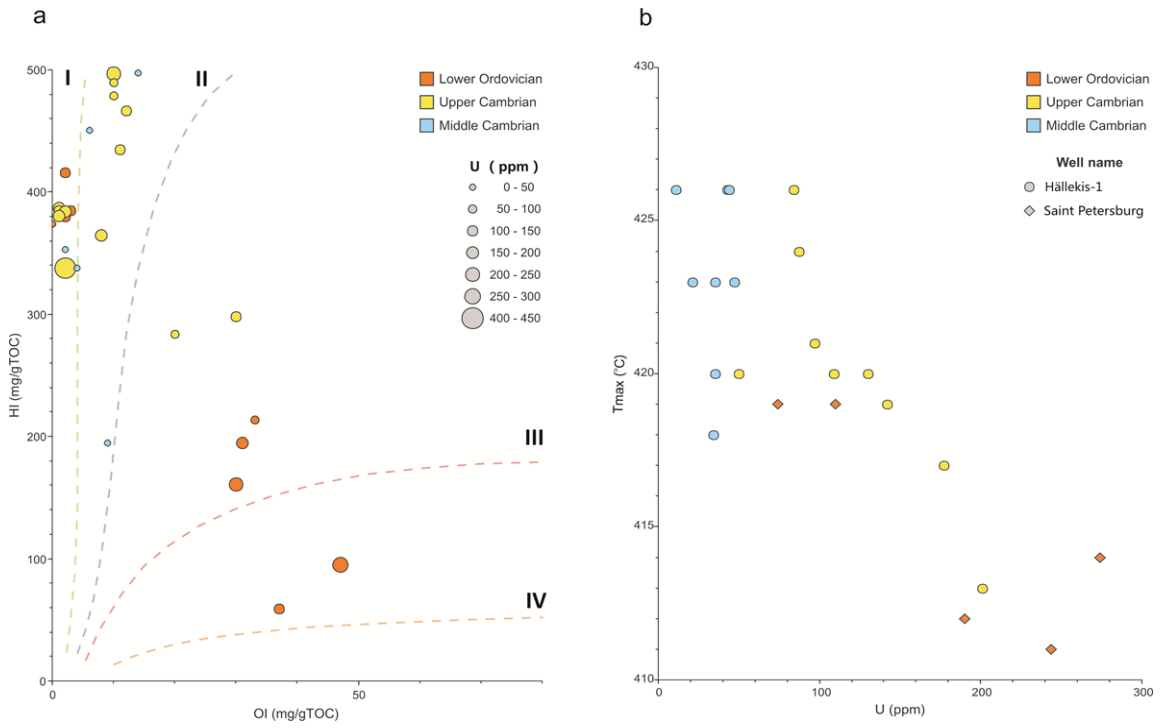


Fig. 2. Correlations between uranium contents and selected Rock-Eval parameters. (a) Different kerogen types can be identified based on the pseudo-van Krevelen diagram (Espitalie et al., 1977). HI and OI are poorly correlated with uranium contents. (b) $T_{max}$ values of samples from two boreholes are generally inversely proportional to their uranium contents.

766 Table 2. Pyrolysis-GC and thermovaporisation-GC data of 16 Alum Shale samples. The ternary end
767 members are normalized as described by Horsfield (1989) and Eglinton et al. (1990). Gas-oil ratios
768 (GOR) gained by Tvap experiment was calculated from gas over resolved oil fractions.

| | Name | Uranium content (ppm) | PyGC | | | | | | Tvap | |
|---|---|---|---|---|---|---|---|---|---|---|
| | | | Horsfield, 1989 | | | Eglinton et al., 1990 | | | GOR | *o*-Xyl/$C_9$ |
| | | | $C_{1\text{-}5}$ Bulk (%) | *n*$C_{6\text{-}14}$ Res.(%) | *n*$C_{15+}$ Res. (%) | 2,3-dmThiophene (%) | *n*-nonene; 9:1 (%) | *o*-xylene (%) | | |
| Lower Ordovician | LO-1 | 74 | 87.5 | 12.5 | 0.0 | 14.2 | 18.8 | 67.0 | 3.2 | 2.6 |
| | LO-2 | 190 | 94.6 | 5.4 | 0.0 | 11.6 | 10.1 | 78.3 | 6.1 | 5.2 |
| | LO-3 | 244 | 96.5 | 3.5 | 0.0 | 12.9 | 6.9 | 80.2 | 5.4 | 9.1 |
| | LO-4 | 274 | 97.4 | 2.6 | 0.0 | 10.5 | 8.1 | 81.4 | 6.9 | 12.7 |
| | LO-5 | 110 | 94.0 | 6.0 | 0.0 | 9.0 | 17.2 | 73.8 | 6.3 | 6.1 |
| | LO-6 | 136 | 91.3 | 8.5 | 0.2 | 8.0 | 18.6 | 73.4 | 5.8 | 3.5 |
| | LO-7 | 107 | 93.3 | 6.7 | 0.0 | 9.0 | 17.6 | 73.4 | 5.9 | 3.7 |
| | LO-8 | 119 | 93.5 | 6.5 | 0.0 | 9.5 | 14.4 | 76.2 | 5.6 | 5.1 |
| | LO-9 | 33 | 78.1 | 20.4 | 1.8 | 6.2 | 54.3 | 39.4 | 0.4 | 0.5 |
| Upper Cambrian | UCm-1 | 155 | 92.5 | 7.3 | 0.2 | 8.5 | 13.4 | 78.1 | 6.8 | 3.2 |
| | UCm-2 | 413 | 98.0 | 2.0 | 0.0 | 9.1 | 5.1 | 85.8 | 6.4 | 12.5 |
| | UCm-3 | 135 | 92.0 | 7.8 | 0.2 | 9.3 | 14.9 | 75.8 | 6.6 | 4.4 |
| | UCm-4 | 186 | 92.4 | 7.4 | 0.2 | 7.3 | 13.2 | 79.5 | 5.5 | 7.5 |
| | UCm-5 | 194 | 94.2 | 5.8 | 0.0 | 10.0 | 10.5 | 79.5 | 4.1 | 8.9 |
| Middle Cambrian | MCm-1 | 14 | 77.0 | 21.0 | 2.0 | 9.5 | 45.3 | 45.2 | 0.8 | 1.8 |
| | MCm-2 | 35 | 79.2 | 18.8 | 2.0 | 13.4 | 39.2 | 47.4 | 0.6 | 1.1 |

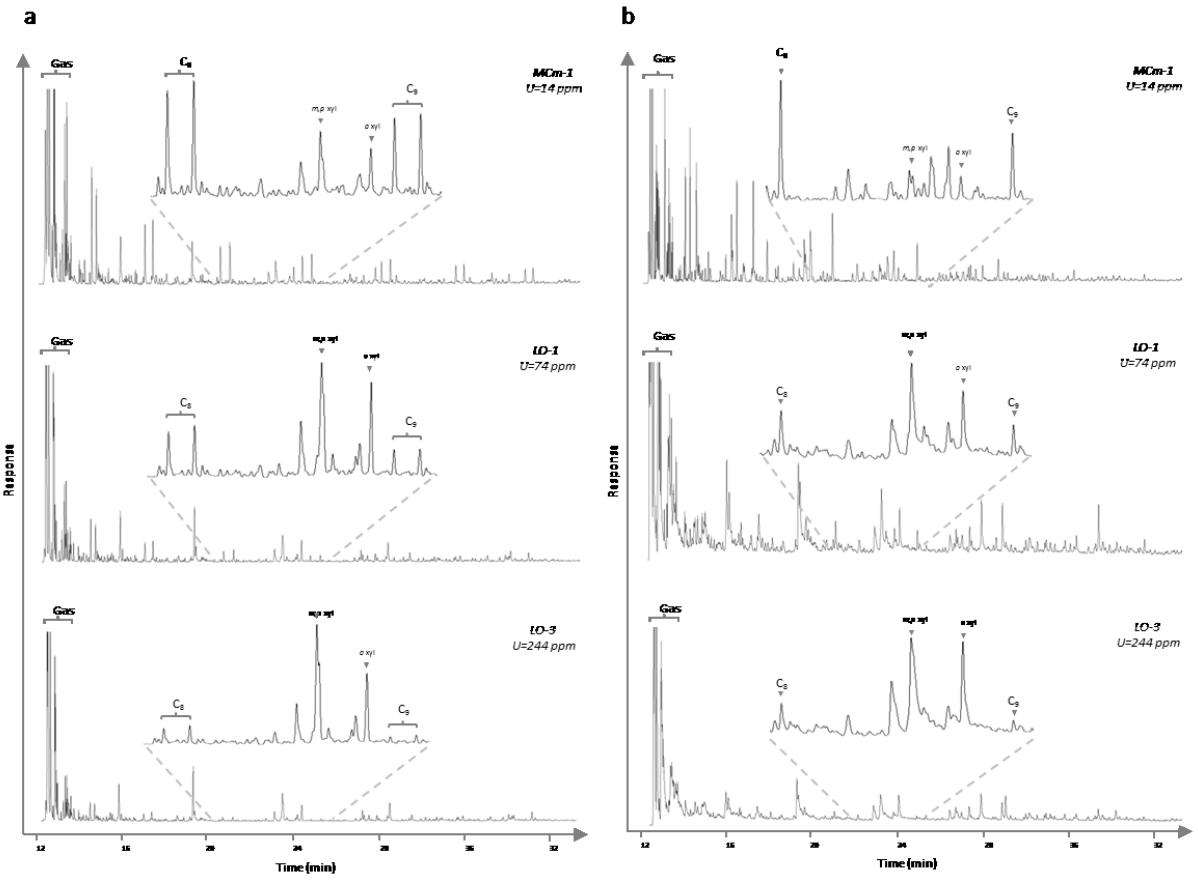


Fig. 3. The pyrolysis- and thermovaporisation-GC traces of three Alum Shale samples with different uranium contents. *n*-alkenes and *n*-alkanes are named by carbon numbers, and major aromatic compounds are illustrated. (a) The pyrolysates show increasing gas/oil ratios and aromaticities in the products with increasing uranium contents from the top to bottom. (b) The Tvap products are featured by the absence of *n*-alkenes compared with pyrolysates of Py-GC, but still show the same trend of compositional changes in response to uranium contents as revealed by pyrolysates.

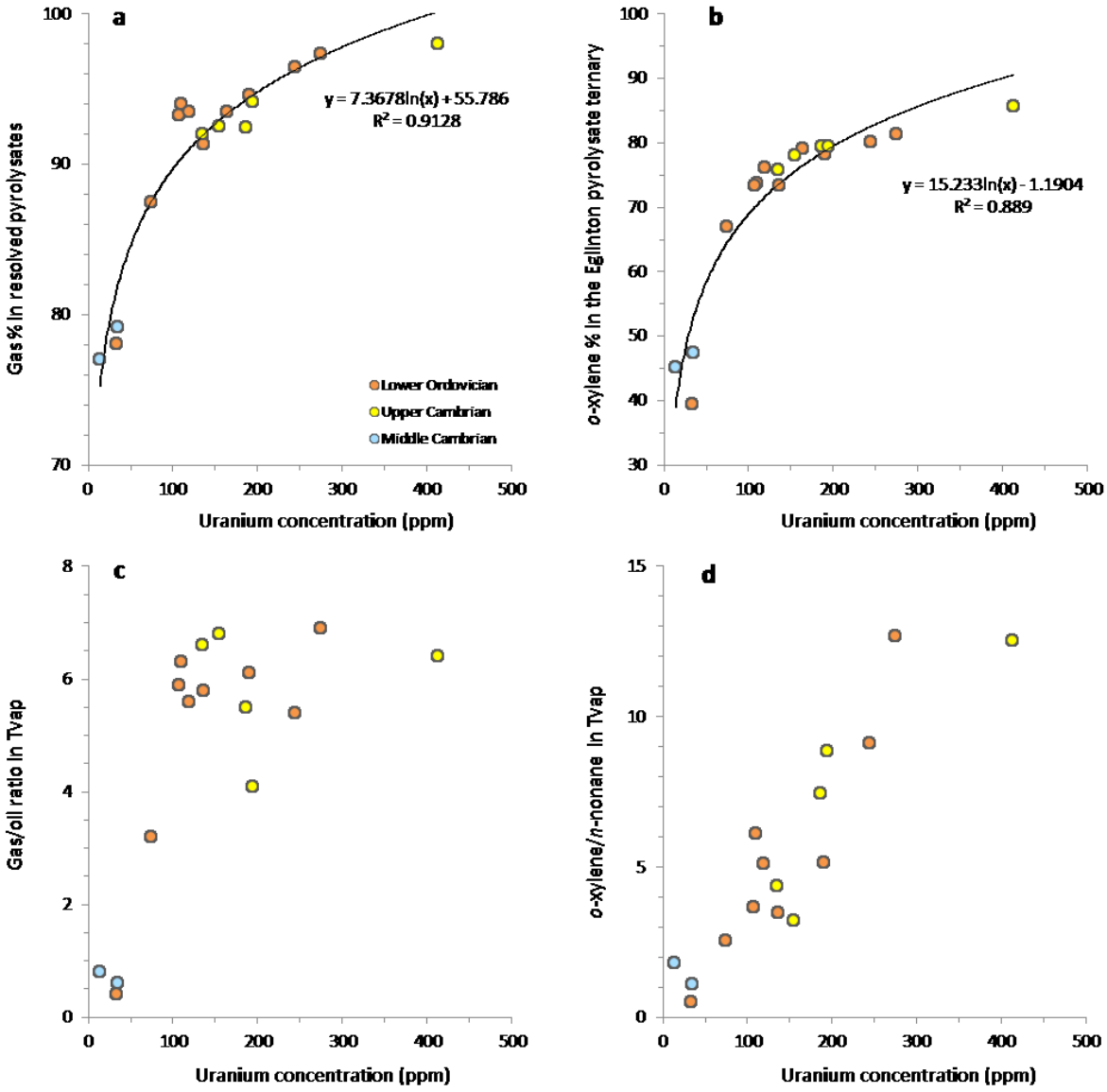


Fig. 4. Correlations between uranium contents with compositional information derived from pyrolysis-GC (a and b) and Tvap-GC (c and d). The gas percentage in (a) and *o*-xylene percentage in (b) are two end members of two classical ternary diagrams as shown in Fig. 5 which are instructive to organic facies. Gas/oil ratio in (c) is calculated from gas/resolved oil in Tvap experiment which reflects the gas richness as in (a). Since the 2,3-dimethylthiophene concentration in Tvap is too low to be accurately interpreted, only *o*-xylene and *n*-nonane were used in (d). Nevertheless, both (b) and (d) allow interpretations about the aromaticity of the products.

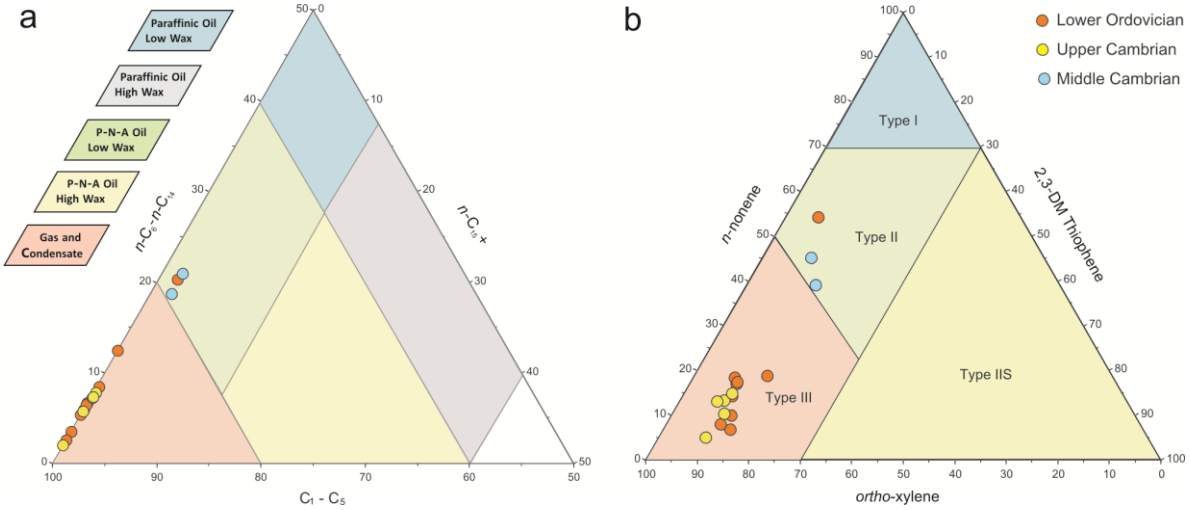


Fig. 5. Ternary diagrams of the pyrolysates for interpretations of organic facies and kerogen structures of the Alum Shale samples (Eglinton et al., 1990; Horsfield, 1989).

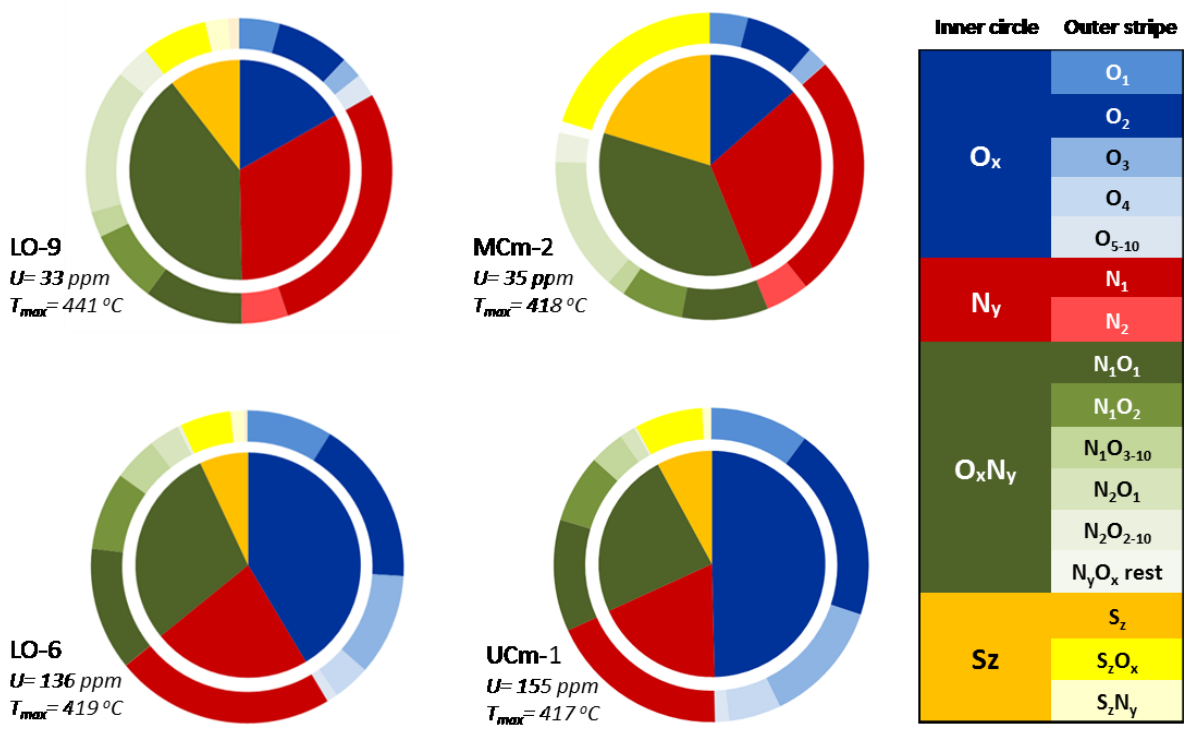


Fig. 6. Elemental class (inner circle) and compound class (outer circle) distribution pie charts of four representative Alum Shale samples derived from ESI (-) FT-ICR MS analyses. Uranium-poor samples (LO-9 and MCm-2) have lower oxygen contents and uranium-rich samples (LO-6 and UCm-1) are characterised by the absence of $N_2$ compounds.

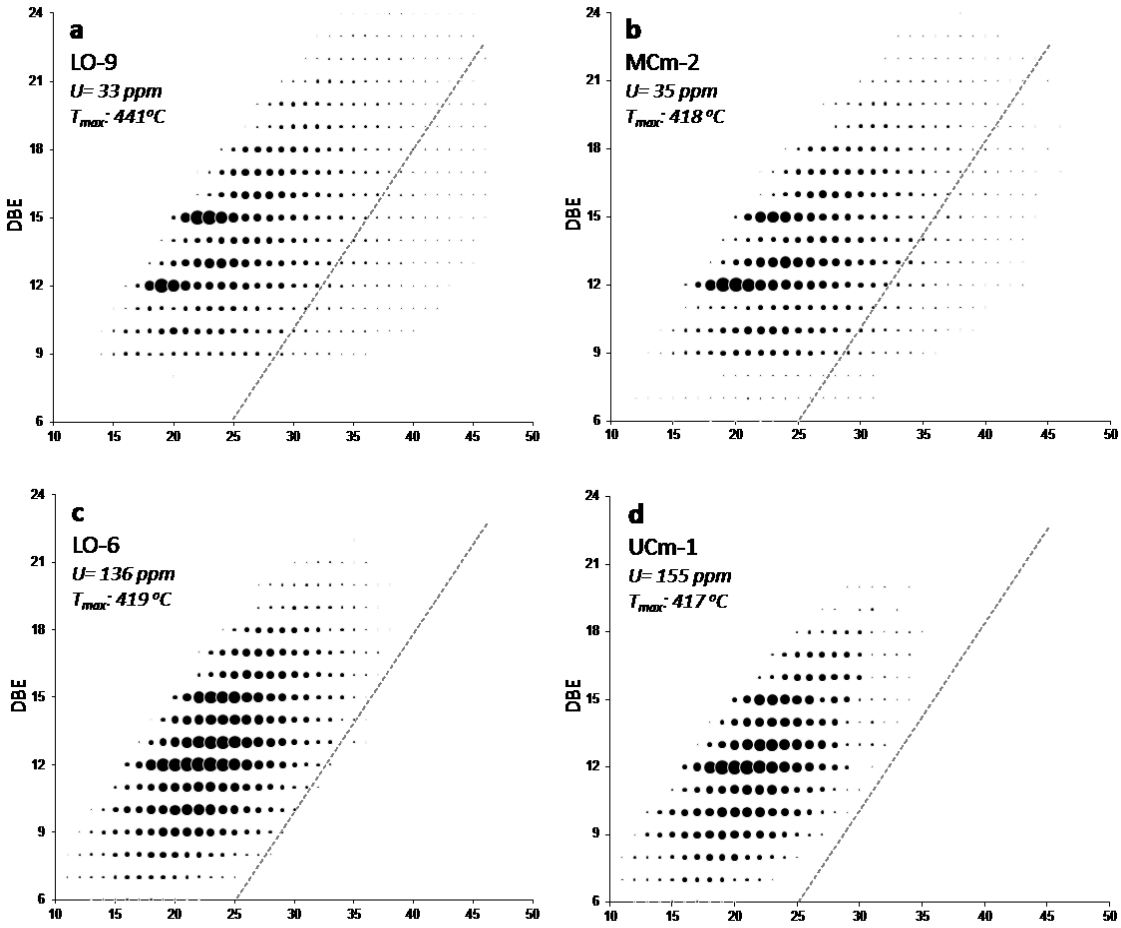


Fig. 7. Double bond equivalent (DBE) against carbon number diagrams on the $N_1$ class of two uranium-poor (a and b) and two uranium-rich samples (c and d). The size of the circles denotes the relative abundance of each compound and the dashed lines on the right hand of each diagram enable comparison of the alkylation.

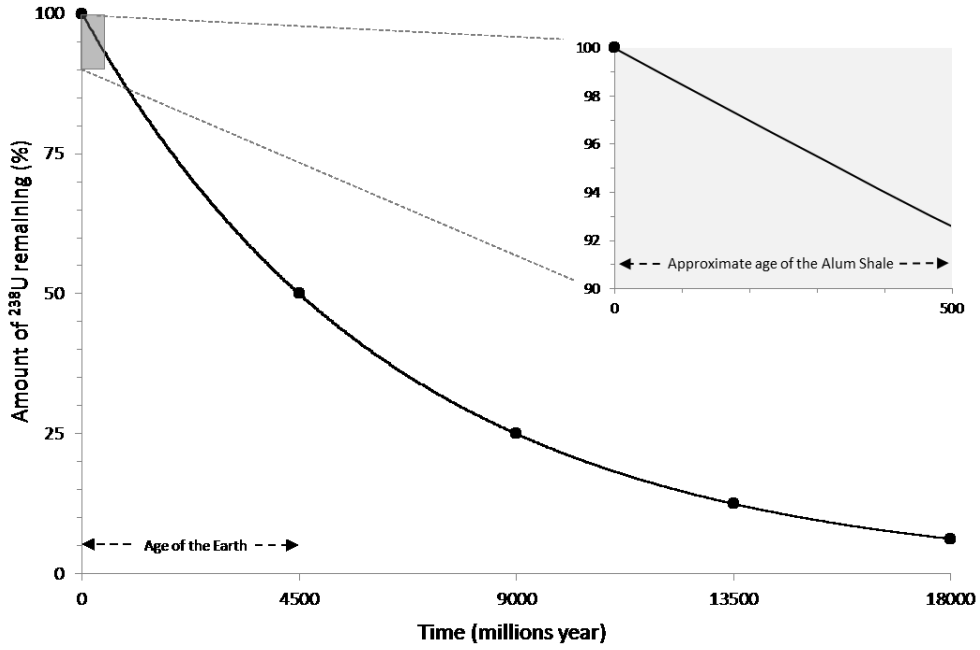


Fig. 8. The exponential decay curve of $^{238}U$. A zoom-in on the geological time scale shows that the decay can be roughly viewed as linearly correlated with time for the Alum Shale.

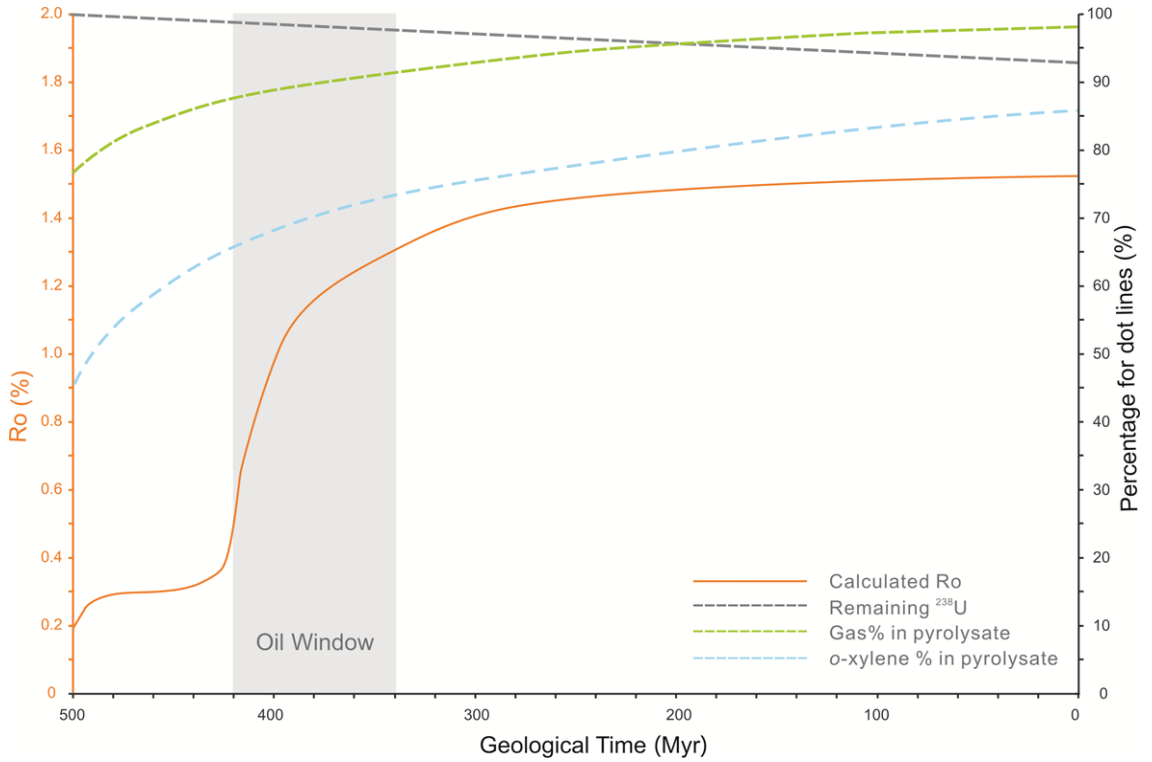


Fig. 9. The back-calculation of products that could be generated from sample UCm-2. Calculated vitrinite reflectance curves are based on basin modelling of well A23-1/88 (location in Fig. 1) from Kosakowski et al. (2010). The oil window was estimated with Ro values between 0.5-1.3 %. The gas and *o*-xylene percentage curves are based on the correlation curves in Fig. 4a and b, respectively. Pyrolysates from sample MCm-1, which has the lowest uranium content and a similar maturity as sample UCm-2, were set as the left end members of these two curves.

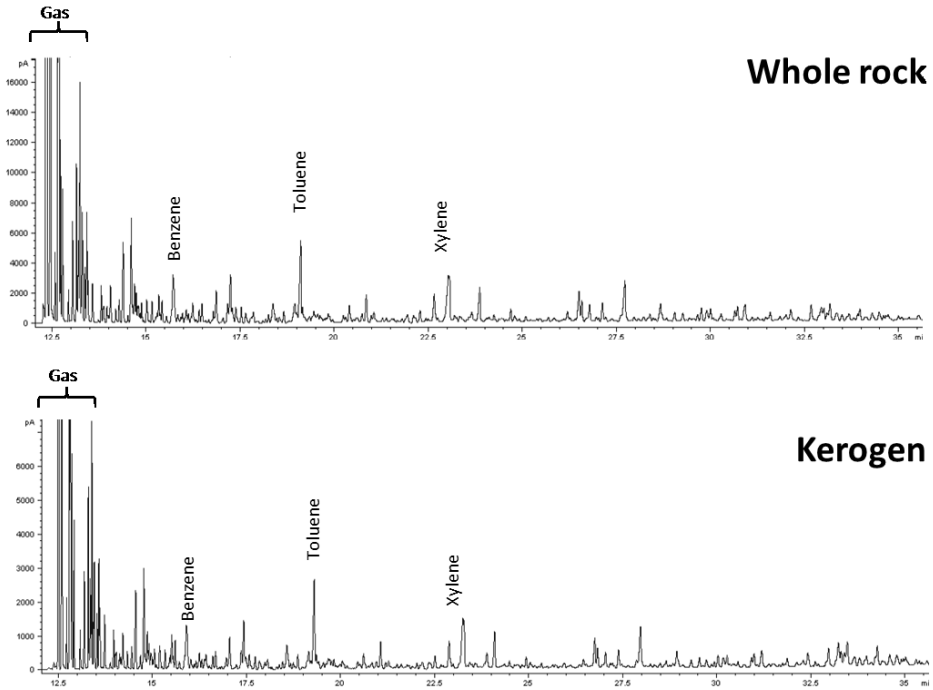


Supplement Figure. Py-GC traces of sample UCm-1 (U=155 ppm) before and after demineralisation. The pyrolysates resemble and imply that the high-gas and high-aromatic production from the Alum Shale were not caused by a mineral catalytic effect.